ISBN: 978-3-95450-227-1 ISSN: 2673-5490 doi:10.18429/JACoW-IPAC2022-WEPOMS005

SIMULATIONS OF THE MICRO-BUNCHING INSTABILITY FOR SOLEIL AND KARA USING TWO DIFFERENT VFP SOLVER CODES

M. Brosi*, P. Schreiber, A.-S. Müller, Karlsruhe Institute of Technology, Karlsruhe, Germany
C. Evain, E. Roussel, C. Szwajj, S. Bielawski, PhLAM - CERLA, CNRS/Lille University, France

Abstract

The longitudinal dynamics of a bunched electron beam is an important aspect in the study of existing and the development of new electron storage rings. The dynamics depend on different beam parameters as well as on the interaction of the beam with its surroundings. A well established method for calculating the resulting dynamics is to numerically solve the Vlasov-Fokker-Planck equation. Depending on the chosen parameters and the considered wakefields and impedances, different effects can be studied. One common application is the investigation of the longitudinal micro-wave and micro-bunching instabilities. The latter occurs for short electron bunches due to self-interaction with their own emitted coherent synchrotron radiation (CSR). In this contribution, two different VFP solvers are used to simulate the longitudinal dynamics with a focus on the micro-bunching instability at the SOLEIL synchrotron and the KIT storage ring KARA (Karlsruhe Research Accelerator).

INTRODUCTION

The longitudinal beam dynamics in a storage ring can be simulated based on the time evolution of the particle distribution in the longitudinal phase space (PS). The evolution of the system can be described by the Vlasov-Fokker-Planck (VFP) equation [1]. Various codes for the evaluation have been written with different methods focussing on different effects. A prominent use-case for the VFP equation, the micro-bunching instability, occurs for short electron bunches due to the self-interaction with the coherent synchrotron radiation (CSR). While it does not lead to beam-loss, it results in non-constant beam parameters. These fluctuations, especially in bunch length and energy spread, may affect the beam quality. At the same time, the increased emission of CSR in the long wavelengths can be utilized for experiments based on THz radiation. VFP solvers also play a vital role in the efforts towards control of this dynamic and providing the possibility for increased and more stable CSR emission or the possibility to suppress the instability [2, 3].

MICRO-BUNCHING INSTABILITY

The interaction of a bunch with its own CSR wakefield results above the instability threshold in substructures forming on the particle distribution in the longitudinal PS (see simulations in Fig. 1). Due to rotation in longitudinal PS these substructures cause continuous changes in the longitudinal bunch profile resulting in temporal fluctuations of the emitted CSR intensity and furthermore change the wakefield. Depending on beam parameters, this dynamic can manifest as the typical saw-tooth shaped bursts in emitted CSR intensity [4, 5]. While the occurrence of substructures is driven by the CSR wakefield, damping and diffusion lead to fillamentation of the structures and causes the bunch to lengthen and the structures to wash-out. This reduces the driving force allowing the bunch to further damp down and become short enough so that the resulting CSR wakefield supports the formation of substructures again. The presence of the micro-bunching instability has been observed at multiple light sources (e.g. [6–12]).

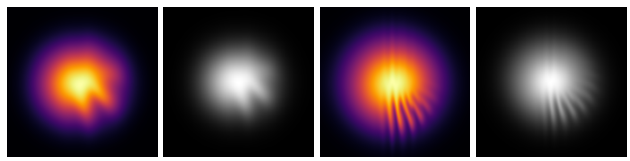

(a) Inovesa (b) PhLAM VFP (c) Inovesa (d) PhLAM VFP

Figure 1: Simulated charge density in the longitudinal PS. (a & b) at 0.26 mA for case **A**, (c & d) at 12 mA for case **C**.

VFP EQUATION & SOLVERS

The Vlasov-Fokker-Planck (VFP) equation describing the evolution of the particle density $\psi(z, E, t)$ with time t can be given by [1, 13, 14]

$$\frac{\partial \psi}{\partial \theta} + \frac{\partial H}{\partial p} \cdot \frac{\partial \psi}{\partial q} - \frac{\partial H}{\partial q} \cdot \frac{\partial \psi}{\partial p} = \beta_\mathrm{d} \frac{\partial}{\partial p} \left(p\psi + \frac{\partial \psi}{\partial p} \right) \quad (1)$$

with the Hamiltonian $H(q, p, t) = H_\mathrm{e}(q, p, t) + H_\mathrm{c}(q, t)$ consisting of the contribution by external fields and the perturbation by collective effects. The coordinates are given as $\theta = f_\mathrm{s} t$ time in synchrotron periods, $q = z/\sigma_{\mathrm{z},0}$ and $p = (E - E_0)/\sigma_{\delta,0}$ as normalised position and energy coordinates with natural bunch length $\sigma_{\mathrm{z},0}$ and energy spread $\sigma_{\delta,0}$. In the radiation damping and quantum diffusion term $\beta_\mathrm{d} = 1/(f_\mathrm{s}\tau_\mathrm{d})$ with the long. damping time τ_d.

The VFP solvers used in this contribution are based on the algorithm derived by Warnock and Ellison [1]. It operates on the charge density discretized in a grid. While the homogeneous solution represents a rotation in PS for the unperturbed case, the influence of diffusion and damping is incorporated as a particular solution.

PhLAM VFP Solver

The VFP solver developed at PhLAM [2, 15, 16] was modelled based on the aforementioned algorithm. The wake-functions for free space and the suppression by parallel plates [17, 18] are directly calculated based on the given input parameters. The necessary convolution of the bunch profile with the wake functions for the wakefield is performed in frequency domain. Therefore, the corresponding impedance is calculated once and multiplied at each time step with the

* miriam.brosi@kit.edu, miriam.brosi@maxiv.lu.se, now at MAX IV Laboratory, Lund

ISBN: 978-3-95450-227-1 ISSN: 2673-5490 doi:10.18429/JACoW-IPAC2022-WEPOMS005

Fourier transformed bunch profile. An inverse Fourier transform of the result giving the wakefield is then applied to the charge density as an additional change in energy. The effects of the Vlasov as well as the Fokker-Planck term are calculated independently and then applied together onto the charge distribution in the longitudinal PS. For both contributions a quadratic interpolation between grid cells is used.

To speed up the calculation the code is parallelized using standard MPI (Message Passing Interface). This enables the simulation to be run in parallel on a cluster, using one or several nodes. Performance tests (speed versus number of cores) can be found in Ref. [19]. The results of the simulation are written to structured text files with a configurable number of simulation steps between data output points. The entire PS can be requested as well and is then written to individual binary files. The program is started from command line and configured by configuration text files. Its various features include, amongst others, the usage of multiple types of bending magnets, additional shot noise, laser interaction and feedback possibilities [2].

Inovesa

The general working principle of Inovesa [14, 20] is similar to the PhLAM VFP solver. However, it directly operates on impedances instead of wake functions. Some impedances such as the parallel plates impedance [17, 21] are directly implemented. The wakefield at each time step is calculated analogously to the PhLAM VFP solver by multiplication of the Fourier transformed bunch profile with the impedance and a subsequent inverse Fourier transform. After the kick in energy due to the wakefield, the rotation due to the Vlasov term is applied split into an energy kick followed by a spatial kick ("Manhattan" rotation [14]). Afterwards, the damping and diffusion described in the Fokker-Planck term are applied. The interpolation between grid cells is cubic by default. Inovesa is parallelized using OpenCL [22] and geared towards the usage on desktop PCs. It can run on multiple CPU cores as well as GPUs. The output makes use of the structuring capabilities of the HDF5 file format [23] and includes derived quantities such as bunch profile or emitted CSR spectrum and on request the full PS density. Inovesa is started via command line and configured either by a configuration file or via command line parameters. An optional live view shows the temporal development of the PS density, emitted CSR intensity, bunch profile and wakefield. Various additional features include noise on the RF voltage and arbitrary impedances from text files. Furthermore, communication during runtime was implemented between Inovesa and e.g. a machine learning agents for control of the instability [24].

EXAMPLES

As example for the comparison of the two simulation codes with respect to the micro-bunching instability, three cases are used (Table 1): **A** SOLEIL at low-alpha, **B** KARA at low-alpha, and **C** SOLEIL at normal-alpha. They represent typical operation modes of SOLEIL and KARA during which the micro-bunching instability is studied [12, 25].

Table 1: Beam Parameters for Simulation Cases

Parameter	**A**	**B**	**C**
Machine	SOLEIL	KARA	SOLEIL
Beam energy / GeV	2.75	1.285	2.75
Bending radius / m	5.36	5.559	5.36
Chamber height (tot.) / mm	25	32	25
RF voltage / MV	2.844	1.048	2.842
Synchrotron freq. / kHz	1.467	8.9	4.64
Bunch length / ps	4.84	4.04	15.31

A common representation of the dynamics during the micro-bunching instability are intensity fluctuation spectrograms. For these, the Fourier transform of the CSR intensity emitted as function of time is displayed as color coded data for a range in bunch current. As the emitted CSR intensity directly depends on the momentary longitudinal bunch profile the observed fluctuation frequencies give an insight into the dynamics of the instability. Figure 2 shows spectrograms for the three example cases simulated with the two VFP solvers.

For the two cases with short bunch length (**A** and **B**) the spectrograms of the simulation results agree very well in overall shape as well as in the features characteristic for the micro-bunching instability. The frequency f_{th} of the dominant fluctuations starting directly above the instability threshold I_{th} is connected to the size of the modulations and the rotations of the charge density [4, 12, 16]. It can be seen for case **A** at 8.9 kHz (PhLAM VFP solver) and at 8.5 kHz (Inovesa). For case **B** it is visible at 32.9 kHz (PhLAM VFP solver) and at 32.6 kHz (Inovesa). The simulated frequency resolution is 0.025 kHz (**A**) and 0.05 kHz (**B**). The good agreement between the codes indicates a similar substructure size in the PS for both simulations (see also Fig. 1a & 1b). Furthermore, as also the fluctuation pattern at higher currents agrees it can be assumed that both simulation codes converge to very similar PS structures as well as dynamics. This is further supported by the agreement in the threshold current. In both cases the codes return the same value, 0.24 mA for case **A** and 0.21 mA for case **B** (with a simulated current resolution of 0.01 mA). A linear scaling law [26] predicting the threshold current exists, for which a good agreement with measurements has been shown [27]. It predicts the threshold current at 0.21 mA and 0.18 mA for **A** and **B** respectively.

In contrast to the previous cases, **C** features a significantly larger bunch length. While the simulations in the first two cases showed a very good agreement between the two codes, the spectrograms (Fig. 2c and 2f) for case **C** show significant differences. On one side, the overall shape does look somewhat similar as both spectrograms show dominant frequency lines above a threshold and at high currents a region with a wide spectrum of fluctuation frequencies. On the other side, there are significant differences in the threshold currents as well as the bunch currents of the transitions between regions with different fluctuation patterns. The threshold currents are 7.6 mA (PhLAM VFP solver) and 6.6 mA (Inovesa) (with a resolution of 0.2 mA). The scaling law predicts a threshold at 5.58 mA. An even bigger difference is visible in the bunch

ISBN: 978-3-95450-227-1 ISSN: 2673-5490 doi:10.18429/JACoW-IPAC2022-WEPOMS005

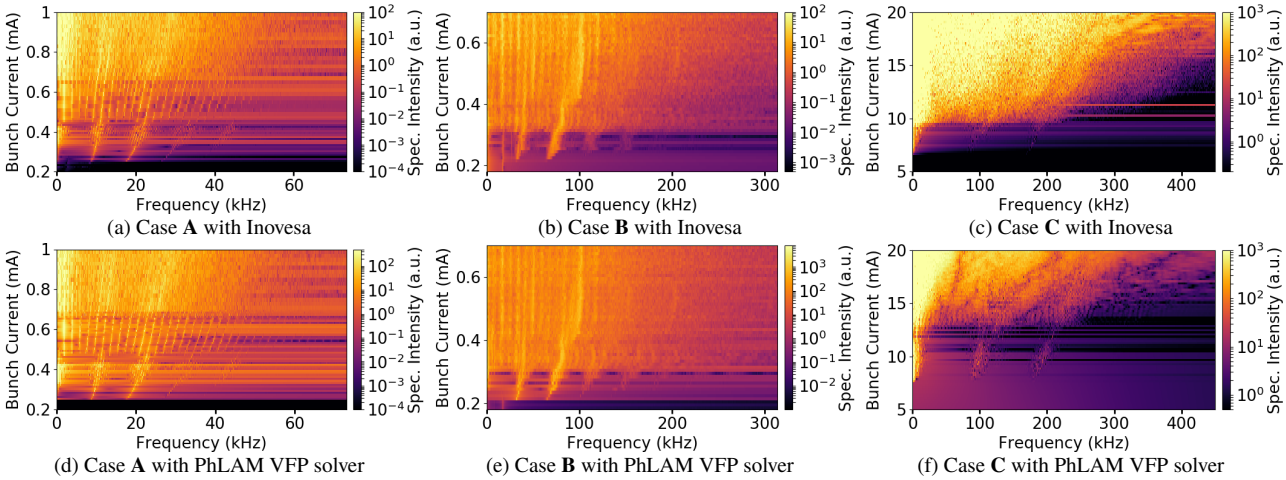

(a) Case **A** with Inovesa (b) Case **B** with Inovesa (c) Case **C** with Inovesa

(d) Case **A** with PhLAM VFP solver (e) Case **B** with PhLAM VFP solver (f) Case **C** with PhLAM VFP solver

Figure 2: Simulated spectrograms of the intensity fluctuations in the emitted coherent synchrotron radiation caused by the micro-bunching instability. For all simulation a grid size of $20\,\sigma_{z,0}$ and $20\,\sigma_{,0}$ with 480×480 bins was used. The simulations were conducted with 8000 steps/4000 steps/2000 steps per synchrotron period for the cases **A/B/C** respectively.

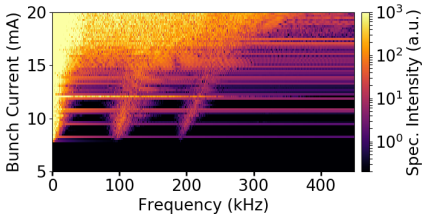

Figure 3: Simulated spectrograms for case **C** with Inovesa with changed rotation style changed from Manhattan to standard and the interpolation reduced from cubic to quadratic.

current where the fluctuation pattern changes from the individual dominant frequency lines to a broader spectrum (PhLAM VFP solver ≈13.0 mA, Inovesa ≈9.6 mA).

In an effort to find the cause of the differences observed for a relatively long natural bunch length (case **C**), the impedances and wakefields were compared and found to agree well between the two codes. Finally, for better comparability of the codes, tests using quadratic instead of cubic interpolation in Inovesa as well as using a standard rotation instead of the Manhattan rotation were conducted. If only one was changed, the results remained the same. But, the combination of a standard rotation with quadratic interpolation ("Inovesa_mod") changed the result drastically (Fig. 3). While, the current where the fluctuation pattern changes is now even higher (14.8 mA), the spectrogram resembles the one from the PhLAM VFP solver (Fig. 2f) more closely.

Independently of which interpolation and rotation is used, f_{th} is similar with 95.5 kHz for Inovesa_mod, 90.6 kHz for the PhLAM VFP solver, and 84.8 kHz for Inovesa in default configuration (simulated frequency resolution of 0.02 kHz), even though the corresponding frequency line is more visible for the PhLAM VFP solver and Inovesa_mod. This indicates, as discussed before, a similar structure size in PS (also see Fig. 1c & 1d) and fits well to the good agreement found between the impedances and wakefields of the two codes.

The used order of interpolation in combination with rotation type, mainly seems to influence the temporal evolution of the growing and shrinking substructures leading to different repetition rates and shapes of the bursts in emitted CSR intensity. This manifests also in the change of the threshold current as well as the current where the fluctuation pattern systematically changes. As this effect was only observed for the simulation at long bunch length, it might be connected to the higher number of substructures in case **C** (see Fig. 1).

SUMMARY

Simulation tools based on solving the Vlasov-Fokker-Planck equation are successfully used to study the longitudinal beam dynamics, and for example the micro-bunching instability. Different implementations exist, two of which, the PhLAM VFP solver and Inovesa, were compared based on example cases for the SOLEIL synchrotron and KIT storage ring KARA. While both codes are based on the same algorithm, they differ slightly in the implementation and use different tools (MPI vs. OpenCL) to allow parallelization. The simulation results for the example with longer bunch length differ between the two codes, especially with respect to the instability threshold as well as the bunch currents at which changes in the instability behavior are observed. It was found that reducing the used interpolation from cubic to quadratic combined with changing the rotation type in Inovesa has a strong effect on the results. However, for the two examples with rather short natural bunch length, the simulations show a very good agreement and seem not influenced by the chosen interpolation and rotation type.

ACKNOWLEDGEMENTS

M.B. acknowledges the funding by the Helmholtz Association in the frame of the Helmholtz doctoral prize. The project has been supported by the ANR-DFG ULTRASYNC project. PhLAM acknowledges support from the CPER Photonics for Society, and the CEMPI LABEX.

ISBN: 978-3-95450-227-1 ISSN: 2673-5490 doi:10.18429/JACoW-IPAC2022-WEPOMS005

REFERENCES

[1] R. L. Warnock and J. A. Ellison, "A General method for propagation of the phase space distribution, with application to the sawtooth instability," in *The physics of high brightness beams. Proc, 2nd ICFA Advanced Accelerator Workshop*, Los Angeles, USA, 9-12 Nov. 1999, published Dec. 2000, pp. 322–348, and http://www-public.slac.stanford.edu/sciDoc/docMeta.aspx?slacPubNumber=SLAC-PUB-8404.

[2] C. Evain *et al.*, "Stable coherent terahertz synchrotron radiation from controlled relativistic electron bunches," *Nature Physics*, vol. 15, no. 7, pp. 635–639, 2019. doi:10.1038/s41567-019-0488-6.

[3] W. Wang *et al.*, "Accelerated deep reinforcement learning for fast feedback of beam dynamics at kara," *IEEE Transactions on Nuclear Science*, vol. 68, no. 8, pp. 1794–1800, 2021. doi:10.1109/TNS.2021.3084515.

[4] M. Brosi, "Overview of the Micro-Bunching Instability in Electron Storage Rings and Evolving Diagnostics," in *Proc. 12th Int. Particle Accelerator Conf. (IPAC'21)*, Campinas, Brazil, May 2021, pp. 3686–3691. doi:10.18429/JACoW-IPAC2021-THXA02.

[5] B. V. Podobedov and R. H. Siemann, "Saw-tooth instability studies in the Stanford Linear Collider damping rings," in *Proc. 17 Particle Accelerator Conf. (PAC'97)*, Vancouver, B.C., Canada, May 1997, pp. 1629–1631. https://accelconf.web.cern.ch/pac97/papers/pdf/2V019.PDF

[6] J. M. Byrd *et al.*, "Observation of broadband self-amplified spontaneous coherent terahertz synchrotron radiation in a storage ring," *Phys. Rev. Lett.*, vol. 89, p. 224 801, 22 2002. doi:10.1103/PhysRevLett.89.224801.

[7] A.-S. Müller *et al.*, "Far infrared coherent synchrotron edge radiation at ANKA," in *Proc. 2005 Particle Accelerator Conf. (PAC'05)*, Knoxville, TN, USA, May 2005, pp. 2518–2520. doi:10.1109/PAC.2005.1591164.

[8] M. Abo-Bakr *et al.*, "Coherent emission of synchrotron radiation and longitudinal instabilities," in *Proc. 2003 Particle Accelerator Conf. (PAC'03)*, Portland, OR, USA, May 2003, paper RPPB006, pp. 3023–3025. https://accelconf.web.cern.ch/p03/PAPERS/RPPB006.PDF

[9] B. E. Billinghurst *et al.*, "Longitudinal bunch dynamics study with coherent synchrotron radiation," *Phys. Rev. Accel. Beams*, vol. 19, p. 020 704, 2 2016. doi:10.1103/PhysRevAccelBeams.19.020704.

[10] W. Shields *et al.*, "Microbunch instability observations from a THz detector at diamond light source," *J. Phys.: Conf. Ser.*, vol. 357, p. 012 037, 2012.]] URL:10.1088/1742-6596/357/1/012037.

[11] Y. Takashima *et al.*, "Observation of intense bursts of terahertz synchrotron radiation at UVSOR-II," *Jpn. J. Appl. Phys.*, vol. 44, no. 35, pp. L1131–L1133, 2005. doi:10.1143/jjap.44.l1131.

[12] C. Evain *et al.*, "Spatio-temporal dynamics of relativistic electron bunches during the micro-bunching instability in storage rings," *EPL (Europhys. Lett.)*, vol. 98, no. 4, p. 40 006, 2012. doi:10.1209/0295-5075/98/40006.

[13] K. Y. Ng, *Physics of intensity dependent beam instabilities*. Hoboken, NJ: World Scientific, 2006, isbn:9789812563422. doi:url10.1142/5835.

[14] P. Schönfeldt *et al.*, "Parallelized Vlasov-Fokker-Planck Solver for Desktop Personal Computers," *Phys. Rev. Accel. Beams*, vol. 20, p. 030 704, 3 2017. doi:10.1103/PhysRevAccelBeams.20.030704.

[15] C. Evain *et al.*, "Direct observation of spatiotemporal dynamics of short electron bunches in storage rings," *Phys. Rev. Lett.*, vol. 118, p. 054 801, 5 2017. doi:10.1103/PhysRevLett.118.054801.

[16] E. Roussel, C. Evain, C. Szwaj, and S. Bielawski, "Microbunching instability in storage rings: Link between phase-space structure and terahertz coherent synchrotron radiation radio-frequency spectra," *Phys. Rev. ST Accel. Beams*, vol. 17, p. 010 701, 1 2014. doi:10.1103/PhysRevSTAB.17.010701.

[17] J. Murphy, S. Krinsky, and R. Gluckstern, "Longitudinal wakefield for an electron moving on a circular orbit," *Particle Accelerators*, vol. 57, pp. 9–64, 1997. http://cds.cern.ch/record/1120287/files/p9.pdf

[18] M. Venturini and R. Warnock, "Bursts of coherent synchrotron radiation in electron storage rings: A dynamical model," *Phys. Rev. Lett.*, vol. 89, p. 224 802, 2002. doi:10.1103/PhysRevLett.89.224802.

[19] E. Roussel, "Spatio-temporal dynamics of relativistic electron bunches during the microbunching instability : study of the Synchrotron SOLEIL and UVSOR storage rings", PhD Thesis, Lille University, France page 51, Sep. 2014. doi:10.13140/2.1.4634.1441,

[20] P. Schönfeldt *et al.*, *Inovesa/inovesa: Gamma two*, 2018. doi:10.5281/zenodo.1321580.

[21] Y. Cai, "Theory of microwave instability and coherent synchrotron radiation in electron storage rings," in *Proc. 2nd Int. Particle Accelerator Conf. (IPAC'11)*, San Sebastian, Spain, Sep. 2011, paper FRXAA01, pp. 3774–3778.

[22] Khronos Group. "Open CL, Open Standard for Parallel Programming of Heterogeneous Systems.", https://www.khronos.org/opencl

[23] The HDF Group. "Hierarchical Data Format, version 5." 1997–2019, https://www.hdfgroup.org/HDF5/

[24] T. Boltz *et al.*, "Feedback Design for Control of the Micro-Bunching Instability based on Reinforcement Learning," in *Proc. 10th Int. Particle Accelerator Conf. (IPAC'19)*, Melbourne, Australia, May 2019, pp. 104–-107. doi:10.18429/JACoW-IPAC2019-MOPGW017.

[25] M. Brosi *et al.*, "Fast mapping of terahertz bursting thresholds and characteristics at synchrotron light sources," *Phys. Rev. Accel. Beams*, vol. 19, p. 110 701, 11 2016. doi:10.1103/PhysRevAccelBeams.19.110701.

[26] K. L. F. Bane, Y. Cai, and G. Stupakov, "Threshold studies of the microwave instability in electron storage rings," *Phys. Rev. ST Accel. Beams*, vol. 13, p. 104 402, 10 2010. doi:10.1103/PhysRevSTAB.13.104402.

[27] M. Brosi *et al.*, "Systematic studies of the microbunching instability at very low bunch charges," *Phys. Rev. Accel. Beams*, vol. 22, p. 020 701, 2 2019. doi:10.1103/PhysRevAccelBeams.22.020701.